liquids

MDPI

Article

Hydrolysis of Al^{3+} in Aqueous Solutions: Experiments and Ab Initio Simulations

Fausta Giacobello [1], Viviana Mollica-Nardo [2], Claudia Foti [1], Rosina Celeste Ponterio [2], Franz Saija [2], Sebastiano Trusso [2], Jiri Sponer [3], Giuseppe Cassone [2,*] and Ottavia Giuffrè [1,*]

1 Dipartimento di Scienze Chimiche, Biologiche, Farmaceutiche ed Ambientali, Università di Messina, Viale F. Stagno d'Alcontres 31, 98166 Messina, Italy; fgiacobello@unime.it (F.G.); cfoti@unime.it (C.F.)
2 Institute for Chemical-Physical Processes, National Research Council of Italy (IPCF-CNR), Viale F. Stagno d'Alcontres 37, 98158 Messina, Italy; mollica@ipcf.cnr.it (V.M.-N.); ponterio@ipcf.cnr.it (R.C.P.); saija@ipcf.cnr.it (F.S.); trusso@ipcf.cnr.it (S.T.)
3 Institute of Biophysics of the Czech Academy of Sciences (IBP-CAS), Kràlovopolskà 135, 61265 Brno, Czech Republic; sponer@ncbr.muni.cz
* Correspondence: cassone@ipcf.cnr.it (G.C.); ogiuffre@unime.it (O.G.)

Abstract: An experimental and computational study on the hydrolysis of Al^{3+} in aqueous solutions is here reported. Speciation model and formation constants were determined by potentiometric titrations at $T = 298.15$ K, $0.1 \leq I/\text{mol L}^{-1} \leq 1$ in aqueous NaCl, $NaNO_3$, $NaCl/NaNO_3$ solutions. The dependence of formation constants on ionic strength is reported in all the ionic media over the range of 0.1–1.0 mol L^{-1}. Under the studied experimental conditions, the formation of $Al_3(OH)_4{}^{5+}$ and $Al_{13}(OH)_{32}{}^{7+}$ species is observed in all the investigated ionic media and ionic strengths. The formation constants of the species formed by Al^{3+} with Cl^- were determined together with the dependence on the ionic strength. Moreover, with the aim of unveiling the molecular structure of the formed Al complexes, quantum-mechanical calculations and state-of-the-art ab initio molecular dynamics simulations under explicit solvation were executed. These computations show, for the first time, the highly cooperative role played by the surrounding water molecules in neutralising mononuclear systems–such as $AlCl^{2+}$ and $AlClOH^+$–and the hydrolytic polynuclear system, $Al_3(OH)_4{}^{5+}$.

Keywords: Al^{3+} hydrolysis; speciation in aqueous solutions; quantum-mechanical calculations; ab initio molecular dynamics; dependence on ionic strengths; potentiometry

Citation: Giacobello, F.; Mollica-Nardo, V.; Foti, C.; Ponterio, R.C.; Saija, F.; Trusso, S.; Sponer, J.; Cassone, G.; Giuffrè, O. Hydrolysis of Al^{3+} in Aqueous Solutions: Experiments and Ab Initio Simulations. *Liquids* **2022**, *2*, 26–38. https://doi.org/10.3390/liquids2010003

Academic Editor: Enrico Bodo

Received: 29 December 2021
Accepted: 2 February 2022
Published: 3 March 2022

1. Introduction

Aluminium is the most abundant metal of the Earth's crust and the third element present after oxygen and silicon. Nonetheless, it is a non-essential element for living organisms, thus resulting detrimental for plants and animals [1–3]. It can achieve an amount of 40 mg in human tissues, causing diseases of skeletal, hematopoietic and nervous central systems [4]. Its wide environmental distribution, deriving from natural and anthropogenic sources, as well as its large usage in disparate applications, has aroused interest in aluminium speciation studies. In aqueous solutions, Al^{3+} establishes strong interactions with water molecules, leading to the formation of hexahydrate complexes. As is well known, Al^{3+} in aqueous solutions exhibits a strong tendency towards hydrolysis, leading to the formation of several mono- and polynuclear hydroxo complexes [5]. In neutral solutions, it precipitates mostly as $Al(OH)_3$, which redissolves with the formation of aluminates, the primary soluble aluminium species at pH > 7. A careful study of the Al^{3+} hydrolysis is quite elusive because of the typical slow reactions occurring in solution and due to interferences stemming from precipitation phenomena. Among the hydrolysis products, it is possible to distinguish mononuclear species—namely, $Al(OH)_r$ ones, with r = 1 . . . 4, which are formed rapidly and reversibly; small polynuclear species—namely, $Al_2(OH)_2{}^{4+}$ and $Al_3(OH)_4{}^{5+}$ ones, which are formed less rapidly and are expected to be quite stable;

large polymeric species, such as $Al_{13}(OH)_{32}{}^{7+}$, which are formed even more slowly and are stable in solution [5]. The current knowledge of Al^{3+} hydrolysis indicates that mononuclear hydroxo species, presumably formed during the initial stages of hydrolysis, readily condense to form polynuclear complexes, in which hydroxo bridges are present between metal centres [6]. Polymeric hydroxo species, which predominate in the complex hydrolysis mechanism of Al^{3+}, are also extensively employed in many areas of material science for the synthesis of new materials and industrial products.

The knowledge of accurate values of hydrolysis constants of Al^{3+} is of crucial importance for the studies on speciation of natural systems, such as natural waters and biological fluids. Al^{3+} hydrolysis has relatively been studied, especially in NaCl, KCl, and $NaClO_4$ and, to a lesser extent, in LiCl, $NaNO_3$, $Ba(NO_3)_2$ ionic media, though not systematically in a wide range of ionic strengths [2,5–13].

As underlined by Sarpola et al., the knowledge of thermodynamic stability constants for polymeric species of aluminium is not completely available [14]. Moreover, polymeric species of Al^{3+} may play relevant roles in different types of processes, such as in the evaluation of the functional mechanisms involved in water treatment, or the ability to increase the rigidity of cell membranes and to cross-link biomolecules, or in geochemistry, for evaluating the formation of minerals. As an example, coagulation has been largely employed in water treatment and wastewater pre-treatment. Among water coagulants, pre-hydrolysed aluminium ion coagulants have been used for this purpose. They are characterised by low residual metal ion concentrations and low residual amounts required for efficiency, attributable to high molecular weights and high cationic charges of polyanionic species of aluminium [15]. Within this context, poly-aluminium chloride sulphates (PACSs) have been employed at various experimental conditions, to improve the coagulating effect of polymerised Al^{3+} species [15].

In the literature, there exist also various studies on the hydrolysis of aluminium, in which techniques such as ^{27}Al NMR spectroscopy [16–23], mass spectrometry [14], Raman spectroscopy [24], IR spectroscopy [17,25], UV spectrophotometry [3,22,26], atomic absorption spectrometry [21,27], and coagulation processes [28] have been used. On the other hand, although some static calculations conducted on relatively small clusters are present in the literature showing the molecular structures of some of the polynuclear hydroxo complexes [17,24,29–31], to the best of our knowledge, no extensive ab initio molecular dynamics (AIMD) simulations explicitly including the contribution of the bulk water solvent have been reported so far.

In the current paper, Al^{3+} hydrolysis is investigated in aqueous NaCl, $NaNO_3$, and $NaCl/NaNO_3$ mixed ionic medium solutions by potentiometry, in the $0.1 \leq I/\text{mol L}^{-1} \leq 1$ range and at T = 298.15 K. It is found that the best speciation model includes the following species: $Al_3(OH)_4{}^{5+}$ and $Al_{13}(OH)_{32}{}^{7+}$. Hydrolysis formation constants of these species in the different ionic media were calculated, and their dependence on ionic strength was also evaluated at T = 298.15 K. Formation constant values of complex species of Al^{3+} with chloride ion were also obtained. Moreover, with aim of shedding light on the microscopic structures formed by chloride and hydroxo aluminium complexes, state-of-the-art quantum-mechanical calculations and ab initio molecular dynamics simulations under explicit water solvation were executed and are here reported.

2. Experimental Section

2.1. Materials and Methods

Aluminium solutions were prepared by weighing the $AlCl_3{\cdot}6H_2O$ salt (Sigma-Aldrich product, Darmstadt, Germany, with purity $\geq$ 99%). Solution concentrations were determined through a back titration, by titrating an excess of EDTA with a $CuSO_4$ standard solution. Sodium chloride and sodium nitrate solutions were prepared by weighing Fluka (Munich, Germany) pure salts previously dried in an oven at 383.15 K. Hydrochloric acid and sodium hydroxide were prepared by using Fluka (Munich, Germany) ampoules and standardised with disodium carbonate and potassium phthalate monobasic, respectively,

dried in an oven at 383.15 K before use. NaOH solutions were stored with soda lime traps to avoid the CO_2 presence inside. For the preparation of each solution, ultrapure water with a conductivity < 0.1 μS cm^{-1}, and grade A glassware were used.

2.2. Potentiometric Equipment and Procedure

All measurements were performed by means of an automatic titration system Metrohm (Herisau, Switzerland) model Dosino 800, a Metrohm (Herisau, Switzerland) LL-Unitrode WOC combined glass electrode and a PC. The titrations were managed through the Metrohm TIAMO 2.2 software, to control the data acquisition, titrant delivery, and emf stability. The estimated accuracy of this system was ±0.15 mV for emf and ±0.002 mL for titrant volume readings. All measurements were carried out into thermostated glass jacked cells (298.15 K ± 0.1 K), under magnetic stirring and bubbling purified nitrogen through the solutions, to prevent O_2 and CO_2 inside. Independent titrations of hydrochloric acid solutions with standard sodium hydroxide were performed to determine the glass electrode potential E^0 and pK_w values, in the same condition of ionic strength and temperature of the system under study.

A solution volume of 25 mL containing aluminium trichloride, hydrochloric acid, and the specific support electrolyte (NaCl or $NaNO_3$ or NaCl/$NaNO_3$ mixture), to reach the desired ionic strength, was titrated with a sodium hydroxide standard solution. Particular attention was given to performing potentiometric measurements on solutions in which sparingly soluble species were present in non-significant amounts. Under the experimental conditions here considered, significant precipitation of sparingly soluble species occurs at pH = 4.5–5. Experimental conditions of the investigations conducted are collected in Table 1.

Table 1. Experimental conditions of the potentiometric measurements at T = 298.15 K.

C_{Al} /mmol L^{-1}	Ionic Medium	C_{Cl}/mol L^{-1}	C_{NO3}/mol L^{-1}	C_{Na}/mol L^{-1}
10–20	NaCl	0.1	—	0.1
10–20		1	—	1
10–20	$NaNO_3$	—	0.1	0.1
10–20		—	1	1
	NaCl/$NaNO_3$			
5–20		0.25	0.25	0.5
5–20		0.25	0.75	1
5–20		0.75	0.25	1
20		0.5	0.5	1

2.3. Calculation Programs for Equilibria in Solution

All parameters of the acid–base titrations (analytical reagent concentrations, electrode formal potential E^0, junction potential coefficient J_a, $E_J = J_a[H^+]$) and the formation constant values were calculated by using the STACO and the BSTAC computer programs [9]. The latter, together with the LIANA software, was employed to study the dependence of the stability constants on the ionic strength [9]. The HySS program was used to draw the distribution diagrams and to calculate the formation percentages of the species [32].

2.4. Quantum-Mechanical Calculations and Ab Initio Molecular Dynamics Simulations

Static quantum-mechanical calculations were performed by means of the Gaussian 09 software [33]. The latter, exploiting quantum-mechanical laws, enables the evaluation of the ground-state structures of selected molecular species. In this study, optimisation of the investigated molecular structures was performed at the second-order of the Møller–Plesset perturbation theory (MP2) [34–37]. Geometry optimisations of the molecular structures were executed under implicit solvation employing the 6-311++G(2d,2p) atomic basis set for all atoms. As far as the simulation of the solvent is concerned, the conductive polarisable continuum model (CPCM) [38] was employed by setting parameters mimicking the water electrostatics. In this way, geometrical relaxations at the ground state of the structures of

two mononuclear systems, $AlCl^{2+}$ and $AlClOH^{+}$, and one hydrolytic polynuclear system, $Al_3(OH)_4{}^{5+}$, were executed.

Additionally to static calculations under implicit solvation, ab initio molecular dynamics (AIMD) simulations—within the Born–Oppenheimer formalism—were performed on 3 numerical samples by means of the CP2K software package [39]. The first one was composed of one $AlCl^{2+}$, 128 water molecules, and 2 Cl^{-} anions (i.e., 388 atoms) placed to neutralise the overall charge of the simulation box. The second numerical sample was composed of one $AlClOH^{+}$, 128 water molecules, and one Cl^{-} (i.e., 389 atoms). The simulation box containing the hydrolytic polynuclear system $Al_3(OH)_4{}^{5+}$ was instead composed of one species of this latter complex, 128 water molecules, and 5 Cl^{-} anions, so as to balance the extra charge carried by $Al_3(OH)_4{}^{5+}$, leading to a total number of atoms equal to 400. In this way, cubic super-cells with edges of 15.82 Å, for both $AlCl^{2+}$- and $AlClOH^{+}$-containing samples, and 16.35 Å for the $Al_3(OH)_4{}^{5+}$-containing one, were simulated. All molecular configurations in the liquid phase were initially set up and pre-equilibrated by means of extensive classical molecular dynamics simulations. Each simulation box was indeed firstly equilibrated via a standard force-field (AMBER) for 1 ns by using periodic boundary conditions. Simulation boxes sizes of these types represent a computational upper bound for ab initio calculations, as discussed in some of the studies recently reported [40–42]. Additionally, periodic boundary conditions were applied along the three Cartesian axes.

Initial atomic configurations of all of the aluminium complexes here investigated were preliminarily structurally optimised at the MP2/6-311++G(2d,2p) level under implicit water solvation conditions, as implemented in the Gaussian 09 code. These optimised structures were successively and separately hydrated with 128 water molecules each, thus forming the cubic simulation boxes mentioned above. During the AIMD simulations, wave functions of each atomic species were expanded in triple-zeta valence plus polarisation (TZVP) basis sets with the Goedecker–Teter–Hutter pseudopotentials [43] using the GPW method. A plane-wave cutoff of 400 Ry was adopted. Exchange and correlation effects were treated via the Becke–Lee–Yang–Parr (BLYP) [44,45] density functional, belonging to the generalised gradient approximation (GGA) class. Moreover, in order to take into account dispersion interactions, which are crucial in correctly simulating the liquid water behaviour and its hydration capabilities, the dispersion-corrected version BLYP-D3 [46,47] was employed. For the sake of coherence with the AIMD simulations, static quantum-mechanical calculations at the BLYP-D3 level and under implicit solvation were also executed, along with those at the higher MP2 level. All AIMD simulations were conducted at the nominal temperature of 330 K. Temperature of the systems was kept fixed through a CSVR thermostat [48] set with a time constant equal to 20 fs. In this way, the systems were kept in an isothermal–isochoric (NVT) ensemble, whereas the nuclei dynamics were classically propagated through the Verlet algorithm with a time-step of 0.5 fs. To gather significant statistics, multiple (i.e., 5) AIMD simulations were performed in parallel by choosing slightly different initial atomic configurations of the aqueous environment, as well as of the initial atomic velocities of the simulated systems. In particular, to obtain almost independent trajectories and monitor the hydration processes in an unbiased manner, pseudo-random initial atomic velocities taken from Maxwell–Boltzmann distributions were assigned. As a consequence, 5 independent 25 ps long AIMD simulations per system were performed, leading to a total simulation time equal to 375 ps (i.e., 3 (simulation samples) × 25 (ps, duration of each trajectory) × 5 (replicas for each system starting with different atomic velocities)). In this way, statistical assessments of the most stable, hydrated complex structures were executed via AIMD simulations.

3. Results and Discussion

Hydrolysis formation constants are expressed according to the following equilibrium:

$$pAl^{3+} + qH_2O \leftrightarrows Al_p(OH)_q{}^{(3p-q)} + qH^{+} \qquad \beta_{pq} \tag{1}$$

A very large number of hydroxo species of Al^{3+} has been reported in the literature. In addition to $Al(OH)^{2+}$, $Al(OH)_2{}^{+}$, $Al(OH)_3{}^{0}$ and $Al(OH)_4{}^{-}$, which predominate at very low Al^{3+} concentrations, $Al_2(OH)_2{}^{4+}$, $Al_2(OH)_4{}^{2+}$, $Al_3(OH)_4{}^{5+}$, $Al_3(OH)_6{}^{3+}$, $Al_4(OH)_2{}^{10+}$, $Al_4(OH)_3{}^{9+}$, $Al_4(OH)_8{}^{4+}$, $Al_7(OH)_{16}{}^{5+}$, $Al_7(OH)_{17}{}^{4+,}$ $Al_{13}(OH)_{32}{}^{7+}$, $Al_{13}(OH)_{34}{}^{5+}$, $Al_{13}(OH)_{35}{}^{4+}$, and $Al_{14}(OH)_{34}{}^{8+}$ were reported under a variety of ionic strengths, ionic media, temperatures, and metal cation concentrations, as shown in Table S1 of the Supplementary Materials. Among these data, the most reported polynuclear species are certainly the $Al_2(OH)_2{}^{4+}$, $Al_3(OH)_4{}^{5+}$, $Al_{13}(OH)_{32}{}^{7+}$ ones.

By considering the potentiometric experimental data, several speciation models, including both mononuclear ($Al(OH)^{2+}$, $Al(OH)_2{}^{+}$, $Al(OH)_3{}^{0}$, and $Al(OH)_4{}^{-}$) and polynuclear ($Al_2(OH)_2{}^{4+}$, $Al_3(OH)_4{}^{5+}$, and $Al_{13}(OH)_{32}{}^{7+}$) species were checked. Under the experimental conditions here explored, polynuclear species appear to be preferred, while mononuclear species, such as $Al(OH)^{2+}$ and $Al(OH)_2{}^{+}$, are not formed in significant amounts. At all ionic strengths and for all of the investigated ionic media, potentiometric data can be well fitted by the speciation model including only two polynuclear hydroxo species, $Al_3(OH)_4{}^{5+}$ and $Al_{13}(OH)_{32}{}^{7+}$. Such a model was then chosen, among other possible models, on the basis of different selection criteria, such as the simplicity (the addition of other, less significant species makes the model unnecessarily complicated), the analysis of the ratios between the variance associated with every single model and that of the selected model, and the comparison between the proposed model and the available data in the literature [49]. Experimental formation constants of the Al^{3+} hydrolytic species, in NaCl, $NaNO_3$, and in $NaCl/NaNO_3$ mixed ionic medium at different ionic strengths and at T = 298.15 K are reported in Table 2. Some experimental values listed in Table 2 ($\log^{T}\beta$ = −13.272, −108.38, for $Al_3(OH)_4{}^{5+}$ and $Al_{13}(OH)_{32}{}^{7+}$, respectively, at T = 298.15 K, and I = 0.167 mol L^{-1} in $NaNO_3$) are fairly close to those reported in the literature ($\log^{T}\beta$ = −13.13, −107.47, for $Al_3(OH)_4{}^{5+}$ and $Al_{13}(OH)_{32}{}^{7+}$, respectively, at T = 298.15 K and I = 0.1 mol L^{-1} in $NaNO_3$) [7,13] (Table S1 in the Supplementary Material). The analysis of the data stemming from the literature confirms that these data are numerous but very fragmentary in the various ionic media.

Table 2. Experimental formation constants of the Al^{3+} hydrolytic species in NaCl, $NaNO_3$, and $NaCl/NaNO_3$ at different ionic strengths, at T = 298.15 K.

Ionic Medium	I [1]	C_{Al} [1]	C_{Cl} [1]	C_{NO3} [1]	$\log\beta_{pq}$ [2]	
					$Al_3(OH)_4{}^{5+}$	$Al_{13}(OH)_{32}{}^{7+}$
NaCl	0.142	0.015	0.11	—	−13.324(3) [3]	−108.48(2) [3]
	0.946	0.015	1.02	—	−13.618(3)	−112.72(1)
$NaNO_3$	0.167	0.015	—	0.16	−13.272(3)	−108.38(1)
	0.963	0.015	—	1.03	−13.320(3)	−110.43(1)
$NaCl/NaNO_3$	0.505	0.012	0.26	0.28	−13.248(4)	−109.88(2)
	0.939	0.012	0.26	0.76	−13.241(5)	−110.62(1)
	0.949	0.012	0.75	0.27	−13.314(3)	−111.30(1)
	0.919	0.02	0.50	0.55	−13.304(7)	−110.97(2)

[1] In mol L^{-1}; [2] refer to the reaction: $pAl^{3+} + qH_2O \leftrightarrows Al_p(OH)_q{}^{(3p-q)} + qH^{+}$; [3] ≥95% of confidence interval.

3.1. Ionic Strength Dependence and Species with Chloride

With the purpose of evaluating the dependence of the formation constants of the hydrolytic species on the ionic strength, the experimental values of Table 2, were analysed by using the following Debye–Hückel type equation [50,51]:

$$\log\beta = \log{}^{T}\beta - 0.51\, z^{*}\frac{\sqrt{I}}{1+1.5\sqrt{I}} + CI \quad (2)$$

where $^{T}\beta$ is the formation constant at infinite dilution; $z^{*} = \Sigma(\text{charge})^2_{\text{reactants}} - \Sigma(\text{charge})^2_{\text{products}}$, whereas C is an empirical parameter. Considering all the experimental hydrolysis constants in various ionic media, it was possible to extrapolate the common values of the hydrolytic

species at infinite dilution along with the different values of the *C* parameter according to the ionic medium. The calculated values of $\log^T\beta$ for the hydrolytic species of Al^{3+} and the *C* empirical parameter are listed in Table 3 for NaCl, $NaNO_3$, and NaCl/$NaNO_3$ aqueous solutions.

Table 3. Formation constants of the Al^{3+} hydrolytic species at infinite dilution, together with the *C* parameter of Equation (2) in NaCl, $NaNO_3$, and in mixed ionic medium (NaCl/$NaNO_3$), at T = 298.15 K.

Species	Ionic Medium	$\log^T\beta_{pq}$ [1]	*C*
$Al_3(OH)_4^{5+}$	NaCl	−13.490(1) [2]	−0.562(6) [2]
$Al_{13}(OH)_{32}^{7+}$		−103.81(6)	−1.75(7)
$Al_3(OH)_4^{5+}$	$NaNO_3$	−13.490(1)	−0.244(6)
$Al_{13}(OH)_{32}^{7+}$		−103.81(6)	0.69(8)
$Al_3(OH)_4^{5+}$	NaCl/$NaNO_3$	−13.490(1)	−0.219(2)
$Al_{13}(OH)_{32}^{7+}$		−103.81(6)	0.1(1)

[1] Refer to the reaction: $pAl^{3+} + qH_2O \leftrightarrows Al_p(OH)_q^{(3p-q)} + qH^+$; [2] ≥95% of confidence interval.

A comparison of the *C* parameter values determined in different ionic media shows that, for $Al_3(OH)_4^{5+}$ species, it is always negative and precisely $C = -0.562$, $-0.244-0.219$ in NaCl, $NaNO_3$, and NaCl/$NaNO_3$, respectively (Table 3). As for the $Al_{13}(OH)_{32}^{7+}$ species, the *C* parameter shows very different values when evaluated in different ionic media.

By means of the values of Table 3, it is possible to obtain the hydrolysis constants at any value of ionic strength in the range investigated.

Speciation diagrams of hydrolytic species of Al^{3+} are shown at I = 0.01, 0.7 mol L^{-1} in NaCl at T = 298.15 K in Figure 1a,b. These ionic strength values were chosen since they correspond to an ionic strength representative of freshwaters and to the average ionic strength of seawaters, respectively. At I = 0.01 mol L^{-1} (Figure 1a) and pH ≈ 4, the $Al_3(OH)_4^{5+}$ species reaches a maximum in the formation percentage of almost 10%; at I = 0.7 mol L^{-1} (Figure 1b) and pH ≈ 4 it increases to almost 30%. $Al_{13}(OH)_{32}^{7+}$ species predominates in the pH range 4–5, reaching a formation percentage of 50% at pH = 4 at I = 0.01 mol L^{-1} (Figure 1a) and at pH = 4.25 at I = 0.7 mol L^{-1} (Figure 1b).

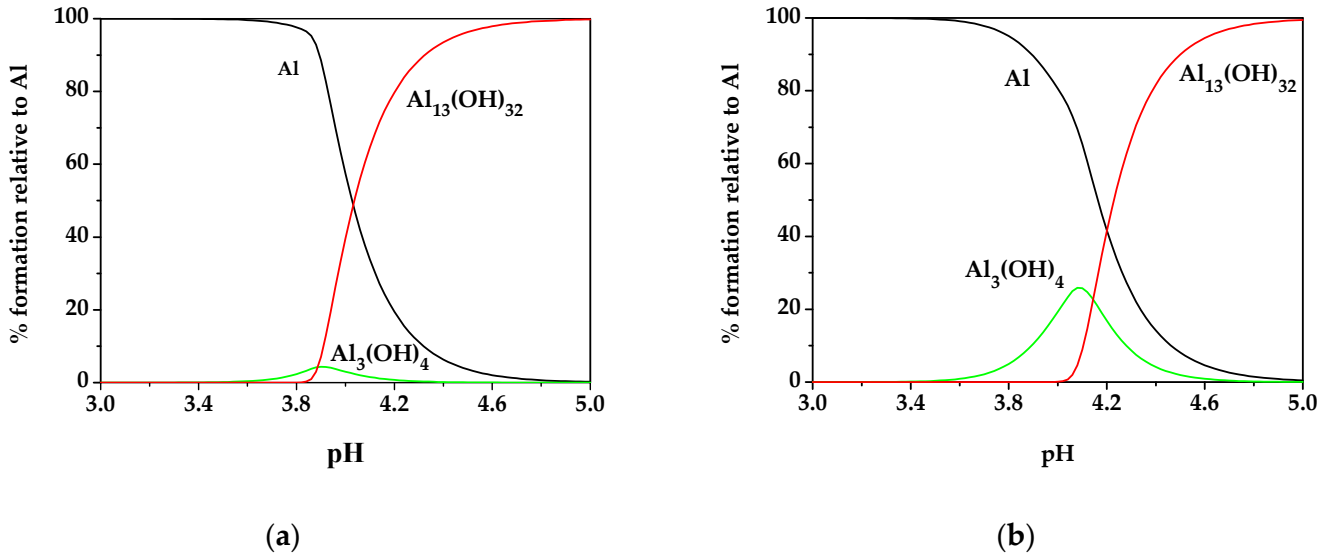

Figure 1. Distribution diagrams of Al^{3+} hydrolytic species at C_{Al} = 20 mmol L^{-1} in NaCl: (**a**) I = 0.01 mol L^{-1}; (**b**) I = 0.7 mol L^{-1}.

The differences in the formation constants in the various ionic media allowed us to quantify the weak interactions of the metal cation with the anion of the ionic medium.

In the current investigation, two species between Al^{3+} and Cl^{-}—namely, $AlCl^{2+}$ and $AlClOH^{+}$, were obtained. Their formation is also supported and characterised by ab initio molecular dynamics (AIMD) simulations under explicit aqueous solvation, as laid out in the following sections. Some examples of experimental and computational synergistic studies were reported in our previous papers [52–54]. Formation constant values of $AlCl^{2+}$ and $AlClOH^{+}$ species, obtained in this investigation are reported in Table 4, together with those of the hydrolytic ones, calculated in aqueous NaCl, $NaNO_3$, $NaCl/NaNO_3$ solutions at T = 298.15 K. To the best of our knowledge, albeit results stemming from density functional theory (DFT) calculations on such an interaction in aqueous solutions are present in the literature, no quantitative thermodynamic data have been reported so far. DFT results indicate that, for Cl^{-}, it is very difficult to enter the inner coordination sphere of Al^{3+} species by replacing the bound water. On the other hand, the structures and behaviour of hydrolysis of Al^{3+} hydroxo species are influenced by Cl^{-} [31].

Table 4. Formation constants for Al^{3+} hydrolytic, chloride species at infinite dilution, together with the C parameter of Equation (2) in different ionic media, at T = 298.15 K.

Species	$\log^{T}\beta$	C [1]
$Al_3(OH)_4{}^{5+}$ [2]	−13.44(2) [3]	−0.23(2) [3]
$Al_{13}(OH)_{32}{}^{7+}$ [2]	−103.89(4)	1.43(8)
$AlCl^{2+}$ [4]	1.33(3)	−0.32(5)
$AlClOH^{+}$ [5]	−3.26(5)	0.26(7)

[1] In NaCl, $NaNO_3$, and $NaCl/NaNO_3$; [2] refer to the reaction: $pAl^{3+} + qH_2O \leftrightarrows Al_p(OH)_q{}^{(3p-q)} + qH^{+}$; [3] ≥95% of confidence interval; [4] refer to the reaction: $Al^{3+} + Cl^{-} \leftrightarrows AlCl^{2+}$; [5] refer to the reaction: $Al^{3+} + Cl^{-} + H_2O \leftrightarrows AlClOH^{+} + H^{+}$.

3.2. Quantum-Based Simulations of Al Complexes in Implicit and Explicit Aqueous Solvents

As explained in detail in the Methods Section, two mononuclear systems, $AlCl^{2+}$ and $AlClOH^{+}$, and one hydrolytic polynuclear aluminium system, $Al_3(OH)_4{}^{5+}$, were structurally optimised under implicit solvation (Figures 2a, 3a and 4a) and subsequently simulated via ab initio molecular dynamics (AIMD) under explicit aqueous solvation (Figures 2b, 3b and 4b). Coordination of the mononuclear species $AlCl^{2+}$ is substantially modified after equilibration in presence of the aqueous solvent treated explicitly (i.e., at the same DFT level of the solute complex). As shown in Figure 2b, the stable chloride complex is surrounded by four additional water molecules. Three of these H_2O species bind the aluminium atom equatorially, whereas the remainder locates in a position which is statistically specular to that of the chloride atom. Such a solvation process leads, among other things, to a weakening and a consequent stretch of the bond formed by the Al and the Cl atoms. In fact, while under implicit solvation, the distance separating these atoms is equal to 2.01 Å at the BLYP-D3 level of theory (Figure 2a), it elongates to an average value of 2.31 Å upon explicit solvation at finite temperature (Figure 2b). Interestingly, the hydrated complex displayed in Figure 2b shows that the three water molecules binding the aluminium atom equatorially are, on average, quite equidistant (≈1.85 Å), whereas the fourth molecule which lies specularly to the Cl atom explores larger distances (≈1.94 Å) from the Al atom.

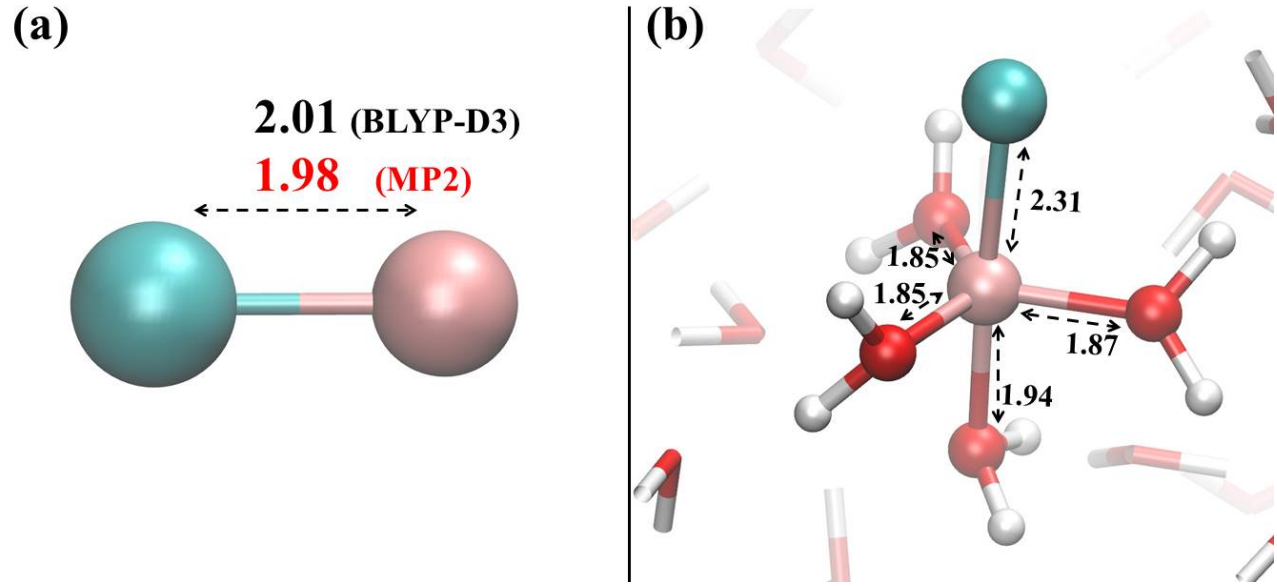

Figure 2. (**a**) Structure of the $AlCl^{2+}$ complex optimised at the MP2/6-311++G(2d,2p) quantum-mechanical level under implicit solvation. The interatomic distance is shown in Å both for the calculation carried out at the MP2 level (red) and for that at the BLYP-D3 level (black); (**b**) structure of the same complex equilibrated upon explicit solvation treatment achieved via ab initio molecular dynamics performed at the BLYP-D3 level. Relevant distances averaged over the last 20 ps of the trajectories are shown in Å.

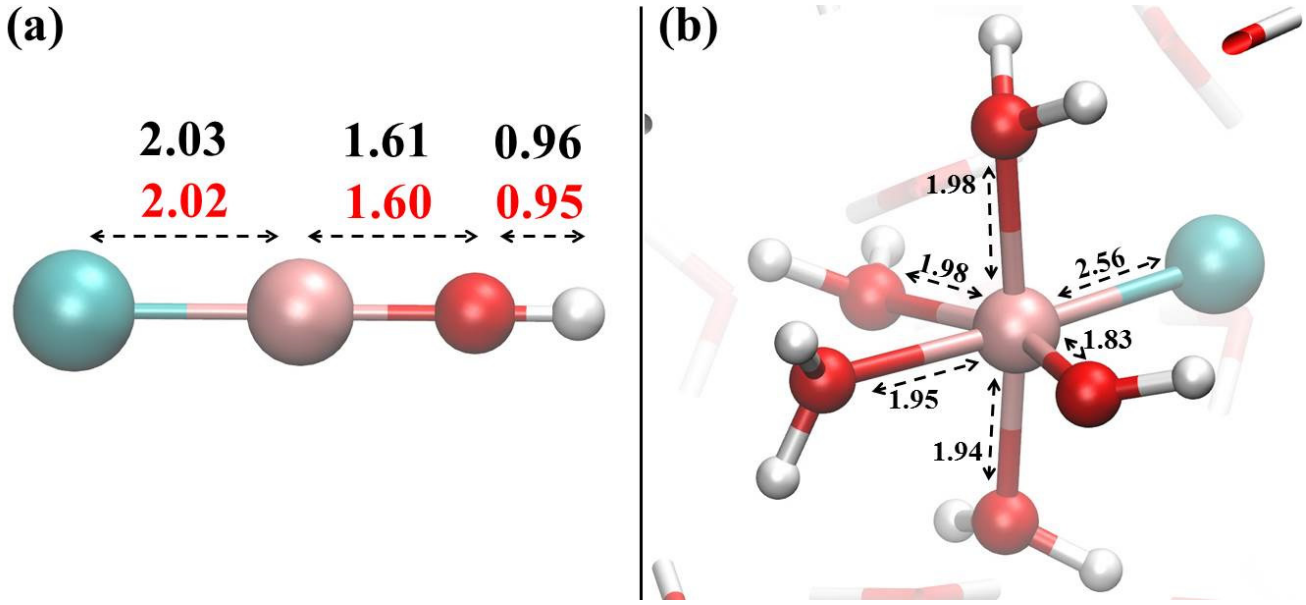

Figure 3. (**a**) Structure of the $AlClOH^{+}$ complex optimised at the MP2/6-311++G(2d,2p) quantum-mechanical level under implicit solvation. Interatomic distances are shown in Å both for the calculation carried out at the MP2 level (red) and for that at the BLYP-D3 level (black); (**b**) structure of the same complex equilibrated upon explicit solvation treatment achieved via ab initio molecular dynamics performed at the BLYP-D3 level. Relevant distances averaged over the last 20 ps of the trajectories are shown in Å.

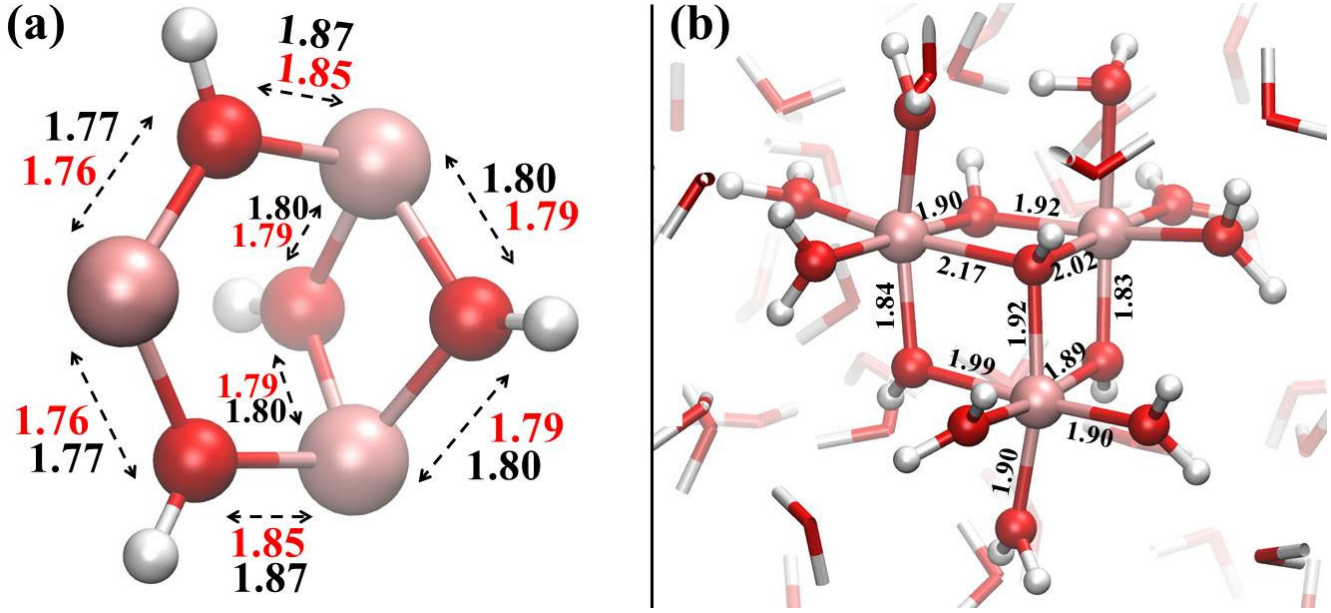

Figure 4. (**a**) Structure of the polynuclear hydroxo $Al_3(OH)_4^{5+}$ complex optimised at the MP2/6-311++G(2d,2p) quantum-mechanical level under implicit solvation. Relevant interatomic distances are shown in Å both for the calculation carried out at the MP2 level (red) and for that at the BLYP-D3 level (black); (**b**) structure of the same complex equilibrated upon explicit solvation treatment achieved via ab initio molecular dynamics performed at the BLYP-D3 level. Some relevant distances averaged over the last 5 ps of the trajectories are shown in Å.

As far as the hydration process of $AlClOH^+$ is concerned, a similar scenario is observed, in that four additional water molecules complete the solvation process of the complex, as shown in Figure 3b. On the other hand, following the hydrolysis reaction of the $AlClOH^+$ complex, the Al-Cl-OH bond angle changes from 180° to ≈100° upon solvation, and the hydroxide anion arranges itself in one of the four equivalent positions around the Al^{3+} ion, as visible from direct comparison of Figure 3a,b. Moreover, the average distance separating the Al and the Cl atoms sizably increases upon solvation. In fact, whilst a value of 2.03 Å is recorded in the ground-state molecular geometry determined at the BLYP-D3 level of theory (Figure 3a), averaging the Al-Cl distance over the last 20 ps of the AIMD trajectories leads to a large value of 2.56 Å (Figure 3b). Such a striking difference (i.e., +26% of elongation of the bond) has certainly to be ascribed to the completion of the solvation process occurring at room temperature. It is noteworthy that the whole solvation mechanism is very fast in the simulated solutions and occurs on timescales shorter than 5 ps, as shown in Figures S1 and S2 of the Supplementary Materials, which show the interatomic distances between the aluminium atom of the original $AlCl^{2+}$ (Figure S1) and $AlClOH^+$ (Figure S2) species with respect to the oxygen atoms of the hydrating water molecules that were monitored as functions of time. All these findings prove, once again, the need for an explicit treatment of the solvent when determining the stable atomistic structures of this type of complexes et similia. Moreover, by employing AIMD simulations, fluctuations of thermal nature are also taken into account, contributing to a better estimate of the enthalpic, in addition to entropic, contributions to the overall stabilisation process.

In accordance with the speciation models that include two polynuclear hydrolytic species, $Al_3(OH)_4^{5+}$ and $Al_{13}(OH)_{32}^{7+}$, as best possible models based on different selection criteria (mentioned above), we constructed a possible cluster containing the four OH^- groups, each of which bridges two metal centres of Al^{3+}. The geometry of such a structure was then optimised, both at the MP2/6-311++G(2d,2p) and at the BLYP-D3/6-311++G(2d,2p) quantum-mechanical levels, as displayed in Figure 4a and reported as a *xyz* structure file in Table S2 of the Supplementary Materials. Interestingly, such an optimised

structure is deeply modified upon solvation. In fact, as shown in Figure 4b, while three of the OH^- anions remain bound to two aluminium atoms, the fourth one increases its own coordination by directly binding all the three aluminium species of the complex, thus forming a form of distorted open cubic structure. Additionally, in this case, interatomic distances change upon solvation, as visible from a direct comparison of Figure 4a,b. However, even though two of the Al-OH bonds are quite weakened upon solvation exhibiting average lengths of 2.17 Å and 2.02 Å, most of the remainder Al-OH bonds do not show elongations larger than the 5% with respect to the implicit solvation case. Global stabilisation of the $Al_3(OH)_4{}^{5+}$ complex is then reached in about 17 ps (Figure S3 in Supplementary Materials) by directly involving nine water molecules (i.e., three per aluminium atom), all pointing toward the first hydration shell of the formed polynuclear complex and located at an average distance of 1.90 Å from the respective Al atoms, which can be formally written as $[Al_3(OH)_4(H_2O)_9]^{5+}$. Such a hydrated complex, similar to the previously discussed ones, appears to be stable—once formed—over the whole AIMD trajectories.

4. Conclusions

In this paper, the hydrolysis of Al^{3+} and the formation of species with chloride were investigated by experiments, quantum-mechanical calculations, and state-of-the-art ab initio molecular dynamics (AIMD) simulations. The formation constants of $Al_3(OH)_4{}^{5+}$ and $Al_{13}(OH)_{32}{}^{7+}$ species were determined by potentiometry in NaCl, $NaNO_3$, and NaCl/$NaNO_3$ aqueous solutions at different ionic strengths. The structure of $Al_3(OH)_4{}^{5+}$, as determined by quantum-mechanical calculations executed at the MP2/6-311++G(2d,2p) level under implicit solvation, shows that each aluminium atom is bound to two hydroxide anions. Moreover, an equivalent structure is also predicted by lower-level density functional theory (DFT) calculations (i.e., BLYP-D3/6-311++G(2d,2p)). By contrast, however, upon explicit solvation achieved by means of AIMD simulations performed at the BLYP-D3 DFT level, such a structure is deeply modified and appears to be coordinated to nine water molecules (3 per Al^{3+} ion) of the local aqueous environment. The formed complex can be formally written as $[Al_3(OH)_4(H_2O)_9]^{5+}$.

The formation constants of $AlCl^{2+}$ and $AlClOH^+$ were also obtained. Although ground-state structures of these latter are linearly arranged, as predicted by quantum-mechanical calculations performed at the MP2/6-311++G(2d,2p) and BLYP-D3/6-311++G(2d,2p) levels and under implicit solvation, four additional water molecules bind the Al^{3+} ion and lead to the stabilisation of the complex upon explicit solvation. Thus, the angle defining the $AlClOH^+$ microscopic structure is deeply distorted from 180° to ≈100° upon solvation and the hydroxide anion arranges itself in one of the four equivalent positions around the Al^{3+} ion. Moreover, the solvation processes of both species lead to a weakening and a consequent stretch of the bond formed by Al and Cl atoms. While in the $AlCl^{2+}$ case, a relative elongation equal to 15% is recorded, a very pronounced increment of 26% of the Al-Cl distance emerges upon solvation of the $AlClOH^+$ species. These findings prove the need for an explicit treatment of the solvent via AIMD simulations when determining the stable atomistic structures of this type of complexes et similia. To this end, crucial fluctuations of thermal nature are also taken into account, contributing to a better reproduction and comprehension of the enthalpic, in addition to entropic, contributions to the overall stabilisation process.

Finally, the formation constants at infinite dilution for the Al^{3+} hydrolytic and chloride species were also reported in the current investigation. These data are essential to obtain constant values at any ionic strength for applications in the field of speciation studies under natural water conditions.

Supplementary Materials: The following supporting information can be downloaded at: https://www.mdpi.com/article/10.3390/liquids2010003/s1, Table S1: Literature data on Al^{3+} hydrolysis, Table S2: *xyz* structure file containing the Cartesian components of the position of the atomic species of the molecular structure of the complex $As_3(OH)_4{}^{5+}$ optimized at the MP2/6-311++G(2d,2p) quantum-mechanical level under implicit solvation (see Figure 4a of the main text). Figure S1: Instantaneous

distances between the aluminium atom of the original $AlCl^{2+}$ species and the oxygen atoms of the four water molecules that hydrate the complex leading to the formation of the structure shown in Figure 2b of the main text, Figure S2: Instantaneous distances between the aluminium atom of the original $AlClOH^{+}$ species and the oxygen atoms of the three water molecules that hydrate the complex leading to the formation of the structure shown in Figure 3b of the main text, Figure S3: Instantaneous distances between the aluminium atom of the original $Al_3(OH)_4{}^{5+}$ species and the oxygen atoms of three of the nine water molecules that hydrate the complex leading to the formation of the complex $[Al_3(OH)_4(H_2O)_9]^{5+}$, whose structure is shown in Figure 4b of the main text.

Author Contributions: Conceptualisation, O.G. and G.C.; investigation, F.G., V.M.-N. and G.C.; resources, O.G., C.F. and J.S.; writing—original draft preparation, O.G., F.G., V.M.-N. and G.C.; writing—review and editing, O.G., G.C., C.F., R.C.P., F.S. and S.T.; supervision, O.G. and G.C.; funding acquisition, O.G. and C.F. All authors have read and agreed to the published version of the manuscript.

Funding: This research was funded by FFABR Unime 2020.

Institutional Review Board Statement: Not applicable.

Informed Consent Statement: Not applicable.

Data Availability Statement: Data is contained within the article or Supplementary Materials.

Acknowledgments: The authors O.G., C.F. and F.G. wish to dedicate this paper to the memory of Prof. Silvio Sammartano. His experience, his in-depth knowledge on this topic, his careful analysis of the potentiometric results, and his helpful discussions were essential for this research.

Conflicts of Interest: The authors declare no conflict of interest.

References

1. Yokel, R.A. Aluminum. In *Elements and their Compounds in the Environment–Occurrence, Analysis and Biological Relevance*, 2nd completely and enlarged edition ed.; Merian, E., Anke, M., Ihnat, M., Stoeppler, M., Eds.; Wiley-VCH: Weinheim, Germany, 2004; Volume 2–Metals and their compounds; pp. 635–658.
2. Kiss, T. From coordination chemistry to biological chemistry of aluminium. *J. Inorg. Biochem.* **2013**, *128*, 156–163. [CrossRef] [PubMed]
3. Parker, D.R. Aluminum speciation. In *Encyclopedia of Soils in the Environment*; Hillel, D., Ed.; Elsevier: Amsterdam, The Netherlands, 2005; pp. 50–56.
4. Yokel, R.A.; McNamara, P.J. Aluminum toxicocinetics: An updated mini-review. *Pharmacol. Toxicol.* **2001**, *88*, 159–167. [CrossRef]
5. Baes, C.F.; Mesmer, R.E. *The Hydrolysis of Cations*; John Wiley & Sons: New York, NY, USA, 1976.
6. Salvatore, F.; Trifuoggi, M. Investigations of Polyoxometalates in Aqueous Solutions. I. The Formation of $Al_{13}(OH)_{32}{}^{7+}$ Cation. *J. Coord. Chem.* **2000**, *51*, 271–282. [CrossRef]
7. Brown, P.L.; Sylva, R.N.; Batley, G.E.; Ellis, J. The hydrolysis of metal ions. Part 8. Aluminium(III). *J. Chem. Soc. Dalton Trans.* **1985**, *9*, 1967–1970. [CrossRef]
8. Cigala, R.M.; De Stefano, C.; Giacalone, A.; Gianguzza, A. Speciation of Al^{3+} in fairly concentrated solutions (20–200 mmol L^{-1}) at I = 1 mol L^{-1} ($NaNO_3$), in the acidic pH range, at different temperatures. *Chem. Spec. Bioavail.* **2011**, *23*, 33–37. [CrossRef]
9. De Stefano, C.; Sammartano, S.; Mineo, P.; Rigano, C. Computer Tools for the Speciation of Natural Fluids. In *Marine Chemistry–An Environmental Analytical Chemistry Approach*; Gianguzza, A., Pelizzetti, E., Sammartano, S., Eds.; Kluwer Academic Publishers: Amsterdam, The Netherlands, 1997; pp. 71–83.
10. Gumienna-Kontecka, E.; Berthon, G.; Fritsky, I.O.; Wieczorek, R.; Latajka, Z.; Kozlowski, H. 2-(Hydroxyimino)propanohydroxamic acid, a new effective ligand for aluminium. *J. Chem. Soc. Dalton Trans.* **2000**, *9*, 4201–4208. [CrossRef]
11. Martell, A.E.; Smith, R.M.; Motekaitis, R.J. *Critically Selected Stability Constants of Metal Complexes. Gaithersburg*; National Institute of Standard and Technology, NIST: Gaithersburg, MD, USA, 2004.
12. May, P.M.; Murray, K. Database of chemical reactions designed to achieve thermodynamic consistency automatically. *J. Chem. Eng. Data* **2001**, *46*, 1035–1040. [CrossRef]
13. Pettit, L.D.; Powell, K.J. *IUPAC Stability Constants Database*; Academic Software, IUPAC: Research Triangle Park, NC, USA, 2001.
14. Sarpola, A.; Hellman, H.; Hietapelto, V.; Jalonen, J.; Jokela, J.; Ramo, J.; Saukkoriipi, J. Hydrolysis products of water treatment chemical aluminium sulfate octadecahydrate by electrospray ionization mass spectrometry. *Polyhedron* **2007**, *26*, 2851–2858. [CrossRef]
15. Gao, B.; Yue, Q. Effect of $SO_4{}^{2-}/Al^{3+}$ ratio and OH^{-}/Al^{3+} value on the characterization of coagulant poly-aluminum-chloride-sulfate (PACS) and its coagulation performance in water treatment. *Chemosphere* **2005**, *61*, 579–584. [CrossRef] [PubMed]
16. Dong, S.; Shi, W.; Zhang, J.; Bi, S. ^{27}Al NMR Chemical Shifts and Relative Stabilities of Aqueous Monomeric Al^{3+} Hydrolytic Species with Different Coordination Structures. *ACS Earth Space Chem.* **2019**, *3*, 1353–1361. [CrossRef]

17. Li, C.; Liu, W.; Ma, Y. Influence of H_3O^+ on the structure formation of oligomers in aluminium sols prepared from basic aluminium acetate: Experiments and computations. *J. Mol. Liq.* **2019**, *289*, 111052. [CrossRef]
18. Maki, H.; Sakatab, G.; Mizuhata, M. Quantitative NMR of quadrupolar nucleus as a novel analytical method: Hydrolysis behaviour analysis of aluminum ion. *Analyst* **2017**, *142*, 1790–1799. [CrossRef] [PubMed]
19. Nýblová, D.; Senna, M.; Düvel, A.; Heitjans, P.; Billik, P.; Filo, J.; Šepelák, V. NMR study on reaction processes from aluminum chloride hydroxides to alpha alumina powders. *J. Am. Ceram Soc.* **2019**, *102*, 2871–2881.
20. Bertsch, P.M.; Thomas, G.W.; Barnhisel, R.I. Characterization of hydroxy-aluminum solutions by aluminum-27 nuclear magnetic resonance spectroscopy. *Soil Sci. Soc. Am. J.* **1986**, *50*, 825–830. [CrossRef]
21. Buffle, J.; Parthasarathy, N.; Haerdi, W. Importance of speciation methods in analytical control of water treatment processes with application to fluoride removal from waste waters. *Water Res.* **1985**, *19*, 7–23. [CrossRef]
22. Feng, X.; Zhang, B.; Lee, C. Effect of low temperature on aluminum(III) hydrolysis: Theroretical and experimental studies. *J. Environ. Sci.* **2008**, *20*, 907–914.
23. Yang, X. Spectroscopy study of aluminium speciation in removing humic substances by Al coagulation. *Water Res.* **1999**, *33*, 3271–3280.
24. Li, N.; Hu, C.; Fu, X.; Xu, X.; Liu, R.; Liu, H.; Qu, J. Identification of Al_{13} on the colloid surface using Surface-Enhanced Raman Spectroscopy. *Environ. Sci. Technol.* **2017**, *51*, 2899–2906. [CrossRef] [PubMed]
25. Su, C.; Suarez, D.L. In situ infrared speciation of adsorbed carbonate on aluminum and iron oxides. *Clays Clay Miner.* **1997**, *45*, 814–825. [CrossRef]
26. Sipos, P.; Capewell, S.G.; May, P.M.; Hefter, G.; Laurenczy, G.; Lukács, F.; Roulet, R. Spectroscopic studies of the chemical speciation in concentrated alkaline aluminate solutions. *J. Chem. Soc. Dalton Trans.* **1998**, *18*, 3007–3012. [CrossRef]
27. Marin, C.; Tudorache, A.; Vladescu, L. Aluminium Determination and Speciation Modelling in Groundwater from the Area of a Future Radioactive Waste Repository. *Rev. Chim.* **2010**, *61*, 431–438.
28. Zhao, H.; Hu, C.Z.; Liu, H.J.; Zhao, X.; Qu, J.H. Role of aluminum speciation in the removal of disinfection by product precursors by a coagulation process. *Environ. Sci. Technol.* **2008**, *42*, 5752–5758. [CrossRef] [PubMed]
29. Li, C.; Liu, W.; Ma, Y. DFT Studies on the Al-Speciation and Its Structure in Aqueous Aluminum Sol Formed by Aluminum Formoacetate. *J. Phys. Chem. B* **2019**, *123*, 9167–9179. [CrossRef]
30. Dong, S.; Shi, W.; Zhang, J.; Bi, S. DFT Studies on the Water-Assisted Synergistic Proton Dissociation Mechanism for the Spontaneous Hydrolysis Reaction of Al^{3+} in Aqueous Solution. *ACS Earth Space Sci.* **2018**, *2*, 269–277. [CrossRef]
31. Jin, X.; Yang, W.; Qian, Z.; Wanga, Y.; Bi, S. DFT study on the interaction between monomeric aluminium and chloride ion in aqueous solution. *Dalton Trans.* **2011**, *40*, 5052–5058. [CrossRef] [PubMed]
32. Alderighi, L.; Gans, P.; Ienco, A.; Peters, D.; Sabatini, A.; Vacca, A. Hyperquad simulation and speciation (HySS): A utility program for the investigation of equilibria involving soluble and partially soluble species. *Coord. Chem. Rev.* **1999**, *184*, 311–318. [CrossRef]
33. Frisch, M.J.; Trucks, G.W.; Schlegel, H.B.; Scuseria, G.E.; Robb, M.A.; Cheeseman, J.R.; Scalmani, G.; Barone, V.; Mennucci, B.; Petersson, G.A.; et al. *Gaussian 09, Revision A.02*; Gaussian Inc.: Wallingford, CT, USA, 2009.
34. Frish, M.J.; Head-Gordon, M.; Pople, J.A. A direct MP2 gradient method. *Chem. Phys. Lett.* **1990**, *166*, 275–280. [CrossRef]
35. Frish, M.J.; Head-Gordon, M.; Pople, J.A. Semi-direct algorithms for the MP2 energy and gradient. *Chem. Phys. Lett.* **1990**, *166*, 281–289. [CrossRef]
36. Head-Gordon, M.; Frish, M.J.; Pople, J.A. MP2 energy evaluation by direct methods. *Chem. Phys. Lett.* **1988**, *153*, 503–506. [CrossRef]
37. Head-Gordon, M.; Head-Gordon, T. Analytic MP2 frequencies without fifth-order storage. Theory and application to bifurcated hydrogen bonds in the water hexamer. *Chem. Phys. Lett.* **1994**, *220*, 122–128. [CrossRef]
38. Tomasi, J.; Mennucci, B.; Cammi, R. Quantum Mechanical Continuum Solvation Model. *Chem. Rev.* **2005**, *105*, 2999–3094. [CrossRef] [PubMed]
39. Kühne, T.D.; Iannuzzi, M.; Del Ben, M.; Rybkin, V.V.; Seewald, P.; Stein, F.; Laino, T.; Khaliullin, R.Z.; Schutt, O.; Schiffmann, F.; et al. CP2K: An electronic structure and molecular dynamics software package–Quickstep: Efficient and accurate electronic structure calculations. *J. Chem. Phys.* **2020**, *152*, 194103. [CrossRef] [PubMed]
40. Previti, E.; Foti, C.; Giuffrè, O.; Saija, F.; Sponer, J.; Cassone, G. Ab initio molecular dynamics simulations and experimental speciation study of levofloxacin under different pH conditions. *Phys. Chem. Chem. Phys.* **2021**, *23*, 24403–24412. [CrossRef] [PubMed]
41. Cassone, G. Nuclear Quantum Effects largely influence molecular dissociation and proton transfer in liquid water under an electric field. *J. Phys. Chem. Lett.* **2020**, *11*, 8983–8988. [CrossRef]
42. Cassone, G.; Creazzo, F.; Giaquinta, P.V.; Saija, F.; Saitta, A.M. Ab initio molecular dynamics study of an aqueous NaCl solution under an electric field. *Phys. Chem. Chem. Phys.* **2016**, *18*, 23164–23173. [CrossRef]
43. Goedecker, S.; Teter, M.; Hutter, J. Separable dual-space Gaussian pseudopotentials. *Phys. Rev. B* **1996**, *54*, 1703–1710. [CrossRef]
44. Lee, V.; Yang, W.; Parr, R.G. Development of the Colle-Salvetti correlation-energy formula into a functional of the electron density. *Phys. Rev. B* **1988**, *37*, 785. [CrossRef] [PubMed]
45. Becke, A.D. Density-functional exchange-energy approximation with correct asymptotic behavior. *Phys. Rev. A* **1988**, *38*, 3098. [CrossRef]

46. Grimme, S.; Ehrlich, S.; Goerigk, L. Effect of the damping function in dispersion corrected density functional theory. *J. Comput. Chem.* **2011**, *32*, 1456–1465. [CrossRef]
47. Grimme, S.; Antony, J.; Ehrlich, S.; Krieg, H. A consistent and accurate ab initio parametrization of density functional dispersion correction (DFT-D) for the 94 elements H-Pu. *J. Chem. Phys.* **2010**, *132*, 154104. [CrossRef] [PubMed]
48. Bussi, G.; Donadio, D.; Parrinello, M. Canonical sampling through velocity rescaling. *J. Chem. Phys.* **2007**, *26*, 014101. [CrossRef] [PubMed]
49. Filella, M.; May, P.M. Reflections on the calculation and publication of potentiometrically-determined formation constants. *Talanta* **2005**, *65*, 1221–1225. [CrossRef] [PubMed]
50. Cardiano, P.; De Stefano, C.; Giuffrè, O.; Sammartano, S. Thermodynamic and spectroscopic study for the interaction of dimethyltin(IV) with L-cysteine in aqueous solution. *Biophys. Chem.* **2008**, *133*, 19–27. [CrossRef] [PubMed]
51. Falcone, G.; Giuffrè, O.; Sammartano, S. Acid-base and UV properties of some aminophenol ligands and their complexing ability towards Zn^{2+} in aqueous solution. *J. Mol. Liquids* **2011**, *159*, 146–151. [CrossRef]
52. Abate, C.; Cassone, G.; Cordaro, M.; Giuffrè, O.; Mollica-Nardo, V.; Ponterio, R.C.; Saija, F.; Sponer, J.; Trusso, S.; Foti, C. Understanding the behaviour of carnosine in aqueous solution: An experimental and quantum-based computational investigation on acid-base properties and complexation mechanisms with Ca^{2+} and Mg^{2+}. *New J. Chem.* **2021**, *45*, 20352–20364. [CrossRef]
53. Cassone, G.; Chillè, D.; Foti, C.; Giuffrè, O.; Ponterio, R.C.; Sponer, J.; Saija, F. Stability of hydrolytic arsenic species in aqueous solutions: As^{3+} vs. As^{5+}. *Phys. Chem. Chem. Phys.* **2018**, *20*, 23272–23280. [CrossRef] [PubMed]
54. Cassone, G.; Chillè, D.; Mollica Nardo, V.; Giuffrè, O.; Ponterio, R.C.; Sponer, J.; Trusso, S.; Saija, F.; Foti, C. Arsenic-nucleotides interactions: An experimental and computational investigation. *Dalton Trans.* **2020**, *49*, 6302–6311. [CrossRef]